Article

In vivo Architectonic Stability of Fully de novo-Designed Protein-Only Nanoparticles

María Virtudes Céspedes, Ugutz Unzueta, Witold Tatkiewicz, Alejandro Sánchez-Chardi, Oscar Conchillo-Solé, Patricia Álamo, Zhikun Xu, Isolda Casanova, José Luis Corchero, Mireia Pesarrodona, Juan Cedano, Xavier Daura, Imma Ratera, Jaume Veciana, Neus Ferrer-Miralles, Esther Vazquez, Antonio Villaverde, and Ramon Mangues

ACS Nano, **Just Accepted Manuscript** • Publication Date (Web): 07 Apr 2014

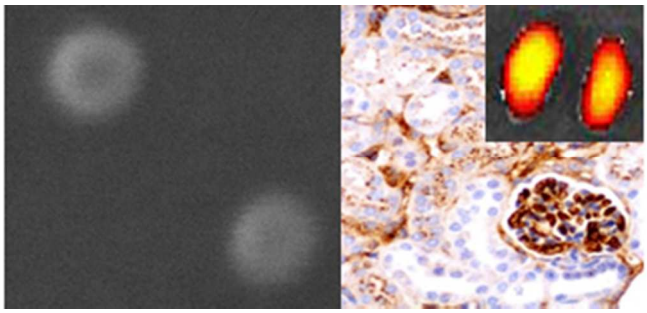

89x39mm (96 x 96 DPI)

In vivo Architectonic Stability of Fully *de novo*-Designed Protein-Only Nanoparticles.

María Virtudes Céspedes[1, 2,] Ugutz Unzueta [2, 3, 4], Witold Tatkiewicz [2, 5], Alejandro Sánchez-Chardi [6], Oscar Conchillo-Solé [3], Patricia Álamo [1, 2], Zhikun Xu [2, 3, 4], Isolda Casanova [1, 2], José Luis Corchero [2, 3, 4], Mireia Pesarrodona [2, 3, 4], Juan Cedano [7], Xavier Daura [3, 8], Imma Ratera [2, 5], Jaume Veciana [2, 5], Neus Ferrer-Miralles [2, 3, 4,] Esther Vazquez [2, 3, 4,] Antonio Villaverde [2, 3, 4*], and Ramón Mangues [1, 2]

[1] Oncogenesis and Antitumor Drug Group, Biomedical Research Institute Sant Pau (IIB-SantPau), Hospital de la Santa Creu i Sant Pau, C/ Sant Antoni Maria Claret, 167, 08025 Barcelona, Spain

[2] CIBER de Bioingeniería, Biomateriales y Nanomedicina (CIBER-BBN), Bellaterra, 08193 Barcelona, Spain

[3] Institut de Biotecnologia i de Biomedicina, Universitat Autònoma de Barcelona, Bellaterra, 08193 Barcelona, Spain

[4] Departament de Genètica i de Microbiologia, Universitat Autònoma de Barcelona, Bellaterra, 08193 Barcelona, Spain

[5] Department of Molecular Nanoscience and Organic Materials, Institut de Ciencia de Materials de Barcelona (CSIC), Bellaterra, 08193 Barcelona, Spain

[6] Servei de Microscòpia, Universitat Autònoma de Barcelona, Bellaterra, 08193 Barcelona, Spain

[7] Laboratory of Immunology, Regional Norte, Universidad de la República, Gral. Rivera 1350, Salto, 50.000, Uruguay

[8] Institució Catalana de Recerca i Estudis Avançats (ICREA), Barcelona, Spain

* Corresponding author: A. Villaverde; antoni.villaverde@uab.cat

Keywords: Protein nanoparticles; Building blocks; Genetic engineering, Biodistribution; Targeting; Drug delivery

Abstract

The fully *de novo* design of protein building blocks for self-assembling as functional nanoparticles is a challenging task in emerging nanomedicines, which urgently demand novel, versatile and biologically safe vehicles for imaging, drug delivery and gene therapy. While the use of viruses and virus-like particles is limited by severe constraints, the generation of protein-only nanocarriers is progressively reachable by the engineering of protein-protein interactions, resulting into self-assembling functional building blocks. In particular, end-terminal cationic peptides drive the organization of structurally diverse protein species as regular nanosized oligomers, offering promise in the rational engineering of protein self-assembling. However, the *in vivo* stability of these constructs, being a critical issue for their medical applicability, needs to be assessed. We have explored here if the cross-molecular contacts between protein monomers, generated by end-terminal cationic peptides and oligohistidine tags, are stable enough for the resulting nanoparticles to overcome biological barriers in assembled form. The analyses of renal clearance and biodistribution of several tagged modular proteins reveal long-term architectonic stability, allowing systemic circulation and tissue targeting in form of nanoparticulate material. This observation fully supports the value of the engineered of protein building blocks addressed to the biofabrication of smart, robust and multifunctional nanoparticles with medical applicability, that mimic structure and functional capabilities of viral capsids.

Nanoparticles; Self-assembling; Architectonic stability; Protein folding; Artificial viruses; Biodistribution

Different types of materials are under examination for the construction of nanoparticles as molecular carriers in diagnosis and therapy, including lipids, diverse types of polymers, dendrimers, carbon nanotubes and metals. [1] While the usage of many of these candidates is technically appealing and their manufacture economically feasible, biocompatibility issues severely compromise *in vivo* applicability. [2] Instead, proteins are ideal biomaterials for therapeutic applications, because of their natural structural roles, easy and cost-effective biological production, functional tuneability by genetic engineering and full biocompatibility. Regarding drug delivery, several categories of entities found in nature support the concept of proteins as ideal nano- or micro-cages for molecular carriage. Infectious viruses, [3,4] virus-like particles (VLPs) [5] and more recently bacterial microcompartments (BMC) [6] and eukaryotic vaults [7] are being explored to transport and deliver nucleic acids, peptides or proteins, chemicals, metals and quantum dots, among others. However, biosafety concerns in the case of viruses and narrow flexibility in re-adapting tropism and geometry in VLPs, vaults and BMCs, stress the need of novel protein nanocages that being highly tuneable and functionally versatile, would not be limited by the above constraints.

The highly organized protein shells of viruses and other natural protein nanocages are formed by self-assembling building blocks that interact through a complex combination of electrostatic, hydrophobic, van der Waals and hydrogen bond forces. [8] So far, the *de novo* design of self-assembling protein monomers for tailored construction has poorly advanced and it is reluctant to generic rational design. [9] Self-assembling amyloidogenic peptides, although showing a wide spectrum of applications in nanomedicine, [9] are unable to generate regular sized shells for controlled drug encapsulation, and their biological fabrication poses important challenges. Concerning full proteins, a limited number of engineering approaches have rendered self-organizing cages or filaments, by adapting oligomerization domains from natural oligomeric proteins, [10,11,12,13] through the *in silico*-assisted fine engineering of protein-protein interfaces [14] or by designing disulfide bonds between cysteine-carrying modified stretches. [15]

Recently [16], we have described a new protein engineering principle for the construction of self-assembling, protein-only nanoparticles, based on the combined use of one cationic peptide plus a polyhistidine. These peptides, fused at either the end termini of recombinant proteins confer tagged monomers (structurally different protein species such as GFP and p53) with a strong dipolar charge distribution that supports

spontaneous self-organization as monodisperse nanoparticulate materials. The size of these particles can be regulated by the ionic strength and specially, by the composition in the cationic residues of the N-terminal tag (larger particle size when tails contain more cationic residues, under a lineal dependence). [16] The N-terminal peptide acts, in addition, as a cell-receptor specific ligand that confers targeting properties to the particle. [16] The relevance of this engineering principle relies on its generic applicability, since contrarily to other proposed approaches it is not limited to any particular protein species and it does not require precise amino acid stretches or composition in the building block to ensure proper assembly, as potentially, any protein can be tagged to promote self-organization. These peptide-driven nanoparticles have been proved useful for the targeted intracellular delivery of proteins [17] and expressible DNA, [18] so far in absence of detectable cellular or organic toxicity. [19]

In particular, the modular protein T22-GFP-H6 was constructed under such tag-based principle, and it forms regular, 13 nm-nanoparticles that internalize, in a particulate form, in CXCR4-expressing cells (T22 being a peptidic ligand of CXCR4 [20]). [19] When administered in metastatic colorectal cancer animal models in which CXCR4 overexpression is clinically relevant, T22-GFP-H6 shows an excellent biodistribution and it is internalized by CXCR4+ cells in the primary tumor and also in the metastatic foci. [16] While this fact is highly promising regarding medical applicability of this platform, it is not clear whether the intermolecular interactions promoted by these nano-architectonic peptides are strong enough to ensure the stability of nanoparticles *in vivo*. In fact, the occurrence of T22-GFP-H6 in target cells and tissues determined by immunohistochemistry does not ensure that the nanoparticulate structure has been maintained during *in vivo* administration. The *in vivo* stability of the nanoparticle formed *in vitro* needs to be confirmed in order to implement this platform as a generic tool for drug design. In fact, if the protein-protein interactions promoted by the peptidic tags are weaker and less complex than those supporting assembling of infectious viruses, VLPs, vaults and BMC shells, it could be not ruled out that the nanoparticles formed *in vitro* by artificial monomers would be immediately disassembled once administered, as the blood stream and intracellular media are rich in charged molecules. In this context, limited stability and a premature release of cargo drugs or imaging agents would fully invalidate the system for further development.

In this regard, determining if a multifunctional protein reaches its target tissue in a nanoparticulate form or as disassembled monomers is not easily approachable experimentally. The *a priori* choice transmission electron microscopy (TEM) does not

offer enough resolution to discriminate between monomeric and nanoparticulate forms (~6 nm *versus* ~13 nm) of protein materials inside target cells (a complex and heterogeneous protein-rich media with similar electrodensity than recombinant proteins), and also between internalized and endogenous protein structures within this size range. Antibodies and gold nanoparticles used in immunolabelling techniques for TEM are also within the same size range. Therefore, we have determined here the *in vivo* architectonic stability of *the novo* designed protein nanoparticles (and therefore, the validity of the whole architectonic principle) by an approach alternative to direct TEM observation that permits a rapid and feasible *in vivo* translation and a refined analysis at the whole body level. This is based on the monitoring of renal clearance and biodistribution of several reporter building blocks (constructs R9-GFP-H6, T22-GPP-H6, T22-IRFP-H6) administered as either monomers (< 7 nm) or assembled entities (> 7 nm). Parental monomeric species as well as closely related protein variants that do not form nanoparticles have been also used as controls. As renal filtration occurs for compounds with a size lower or around 7 nm, [21] accumulation of the administered material in kidney but not in target tissues would be indicative of disassembling, while occurrence in target tissues but not in kidney would prove the *in vivo* stability of nanoparticles. Interestingly, the obtained results indicate that nanoparticles formed *in vitro* are highly stable during systemic circulation, thus proving the structural robustness and strong potential of end terminal cationic tags as nano-architectonic tools for medical applications.

Results and discussion

The fusion of N-terminal cationic peptides to H6-tagged GFP promotes the self-organization of the construct into protein-only nanoparticles of sizes ranging from 10 to 50 nm. [16] These particles are immediately observed upon protein purification from recombinant bacteria and they probably assemble in the storage buffer against which the protein is dialyzed after elution. Being highly cationic, peptides R9 and T22 (used in nanomedicine for brain targeting and $CXCR4^+$ cell targeting respectively, Figure 1 A) support the self-assembling of GFP-H6 as fully fluorescent particles of ~20 nm and ~13 nm (Figure 1 B). The sizes of these particles, primarily determined by DLS, were confirmed by TEM (Figure 1 C) and AFM (Figure 1 D, and Supplementary Figures 1 and 2). In contrast, the non-cationic peptides Ang-and Seq fail in promoting any supramolecular organization of the fusion proteins, and the size of the monomers was coincident in both cases with that of GFP-H6 (around 6 nm, Figure 1 B).

In mice, upon single intravenous (i.v.) administration at equal doses, Ang-GFP-H6, Seq-GFP-H6 and the parental GFP-H6 accumulated in kidney (Figure 2 A, B, C), indicative of renal clearance and in agreement with the occurrence of these proteins in a monomeric form also *in vivo*. Contrarily, R9-GFP-H6 and T22-GFP-H6 were not observed in kidney (Figure 2 A, B, C), suggesting that the nanoparticulate architecture reached by these proteins *in vitro* (Figure 1 C, D) was maintained *in vivo* during circulation in blood. No protein was detected in lung, heart, spleen or liver in any case (Figure 2 A). Consistently with their lack of renal clearance the fluorescence emitted by R9-GFP-H6 and T22-GFP-H6 was detectable in plasma showing a first fast half-life of rapid distribution in the blood compartment, followed by a second and slow half-life of long-lasting permanence in blood (Figure 2 D, and Supplementary Table 1). Leucocytes and platelets showed lack of fluorescence accumulation for R9-GFP-H6, whereas fluorescence after T22-GFP-H6 administration was slightly increased in these blood cells as compared to background fluorescence in non-accumulating tissues, but it was till 100 times lower than fluoresce reached by T22-GFP-H6 in tumor tissue. No accumulation was observed in red blood cells (Supplementary Figure 3). Although *a priori* it could be not discarded that the absence of protein in kidney would be due to a proteolytic instability and fast degradation, T22-GFP-H6 was observed to be highly stable in plasma and when administered to colorectal cancer mice models it accumulated in primary tumors and metastatic foci. [19] The combination of all these data was indicative that the protein reached its target in a full-length form. In this particular construct, the N-terminal peptide T22 was at the same time an architectonic tag and a

cell-specific ligand, as it binds the cell surface receptor CXCR4 and internalizes $CXCR4^+$ cells. [19,20] Interestingly, no enhancement of apoptosis was observed in any of the checked organs, namely non-tumoral lung, heart, spleen and liver (Supplementary Figure 4), and no loss of weight or other pathological signs of toxicity were observed in any of the administered animals as compared to vehicle-treated animals (not shown). The absence of cellular toxicity of T22-GFP-H6 *in vitro* had been already reported, [19] altogether indicating a potential of these protein particles for *in vivo* applications.

To complement these data, we first confirmed the proteolytic stability of R9-GFP-H6 and related monomeric proteins in plasma and serum (Figure 3 A), that was as high as that observed in T22-GFP-H6. [19] Then, the biodistribution analysis of R9-GFP-H6 upon administration determined that this protein nanoparticles localized in brain (a background occurrence of GFP-H6 was also determined; Figure 3 B, C). This was not completely unexpected as previous findings suggested a BBB-crossing potential of R9 and related arginine rich peptides. [22,23] Since neither R9- nor T22-empowered proteins were detected in lung or heart (Figure 2 A), the possibility of unspecific protein aggregation can be strongly excluded, whereas the lack of accumulation in spleen or liver indicate that they are not taken by the mononuclear phagocyte system that affects other categories of nanoparticles. [24,25] Again, the absence of these proteins in kidney must be exclusively attributed to their nanoparticulate organization that prevents size-dependent clearance. Renal filtration of parental GFP-H6 and related non-assembling proteins also indicated that these constructs, with a size very close to the threshold for filtration, do not tend to aggregate or assemble *in vivo* and that they keep their monomeric form during circulation in blood.

While offering an enormous potential in the design of artificial viruses and protein nanoparticles for medical purposes, [26] the high *in vivo* architectonic stability of R9-GFP-H6 and T22-GFP-H6 observed here was not anticipated. Being R9 and T22 highly cationic and the whole chimerical constructs showing a dipolar charge distribution [16] we expected electrostatic charges being the main drivers of protein assembly. Then, nanoparticle stability in media with a high load of charged components, such as bloodstream (negatively charged proteins and a wide catalogue of ions) was at least initially surprising, as we could presume molecular competitions between charged agents and building blocks and consequent particle dissociation. Experimental data indicated, instead, that nanoparticles formed *in vitro* keep such organization also *in vivo*. To test this 'structural memory' we evaluated renal clearance of a novel modular protein generated in this study (T22-IRFP-H6). In this construct, the core of the building

block is iRFP, a dimeric fluorescent protein with primary sequence and structure unrelated to those of GFP. Once purified in low salt buffer, this construct self-organizes as nanoparticles of ~14 nm (Figure 4 A, B) while it remains disassembled (probably as natural dimers) in high salt buffer (Figure 4 A). Furthermore, adding salt to the protein when already assembled in low salt buffer (to reach the same salt concentration than in high salt buffer) does not alter particle size (Figure 4 C). This is indicative of a tight organization of the protein assemblies and of robust cross-molecular interactions between monomers that are not responsive to alterations of the media conditions upon assembling. In this context, NP40 had also no effect on the stability of nanoparticles (Figure 4 D) while the strong denaturant detergent SDS used as a control disassembled the constructs already at 0.1 % (Figure 4 E). The progressive reduction of the protein size observed at 0.1 and 1 % could reflect a hierarchical disassembly of nanoparticles first releasing dimeric T22-IRFP-H6 building blocks and later individual denatured monomers.

To assess more robustly the *in vivo* stability and architectonic memory of protein nanoparticles we administered the polypeptide T22-IRFP-H6 to colorectal cancer mice models, either in disassembled (high salt buffer) or assembled (low salt buffer) forms. Upon i.v. injection, renal clearance was observed only in the case of the disassembled protein, while tumor targeting was only observed in the nanoparticulate form (Figure 5 A, B). This fact indicated again the preservation in the bloodstream of the molecular organization adopted *in vitro,* but also it proved that tissue targeting by efficient cell surface ligands is impaired by renal clearance, as it prevents individual proteins reaching the intended target. Presentation of the failing polypeptide in a nanostructured form with a size higher than 7 nm instead avoids renal excretion and it confers a high recirculation time in blood, thus offering opportunities for its accumulation in the target tissue. Importantly, since the cell ligand is the peptide T22 in both cases, no biased biodistribution could be potentially attributed to the use of different ligands but exclusively to the presentation in disassembled or assembled forms.

To explore the fine architecture of these nanoparticles we fist estimated the number of monomers forming them, by size-exclusion chromatography. Interestingly, the 23 nm R9-GFP-H6 particles peaked out of the column range, but still, an important fraction peaked at a value compatible with a pentameric organization of the protein, in agreement with previous *in silico* modeling. [16,18,19] There, the basic structure of R9-GFP-H6 nanoparticles has been suggested to be star-shaped discoidal pentamers, in which monomers are organized as a ring around an empty center. [18] On the other

hand, T22-GFP-H6 and T22-IRFP-H6 were majorly organized in clusters of ten monomers (Figure 6 A), but minor peaks corresponding to fifteen T22-IRFP-H6 monomers, to the T22-IRFP-H6 dimer (the natural form of IRFP) and to T22-GFP-H6 monomers were also observed. The occurrence of oligomers formed at least by five, ten and fifteen monomers would account for the slight polydispersion of the particle size determined by DLS (Figure 1 B) and strongly suggested the stacking of basic pentameric blocks in higher order structures. In this regard, the tubular organization observed in R9-GFP-H6-DNA complexes [27] is again fitting with a model in which nanodisks are piled as cylinders. The robustness of the emission spectra of assembled GFP variants when compared with regular GFP (Figure 6 B) indicated little or no conformational changes in the GFP barrel associated to nanoparticle formation. In this context, the overhanging tails (R9 or T22 and H6) rather than the monomer core itself could be the main responsible for protein-protein interactions in the nanoparticle, as previously suggested. [16,18] In a last structural analysis, Cryo-TEM and especially high resolution FESEM (Figure 6 C) showed a ring shaped organization of all protein particles that in the case of T22-GFP-H6, would be compatible with two staked pentamers. These new data confirmed again the particle sizes determined primarily by DLS and AFM (Figure 1 and Supplementary Figure 1 and 2) and the circular distribution of the protein material (Figure 6 C).

All these results clearly indicate that once nanoparticles are formed, their architecture remains stable both *in vitro* and *in vivo*, and that while salt content modulates the initial configuration of protein-protein interactions it does not disturb the structure of the formed supramolecular complexes. The cross-molecular contacts between monomers would be then more complex than mere electrostatic interactions and probably similar to those occurring in viruses and related entities. At a neutral pH, the poly-histidine tail is not charged, and the interaction between arginines and neutral histidines is known to be strong, as it may combine polar, hydrophobic and cation-pi (between the guanidinium positive charge and the aromatic imidazole ring) interactions. These interactions may be favorable even when H6 is positively charged, as expected under slightly acidic environments. [28,29]

Because of the especially high definition of ring-shaped FESEM images and the occurrence of pentameric structures in R9-GFP-H6 nanoparticles, we modeled protein-protein interactions in this particular construct [16,18]. Different probable star-shaped nanoparticles resulted from the docking process depending on the conformation adopted by the overhanging end terminal peptides, all of them in the range of 15-30 nm

and compatible with the nanoparticle size (Figure 7). When resolving the energetics organizing the monomers, complex combinations of electrostatic interactions, van der Waals forces and hydrogen bonds were found in all cases (Table 1), as in those occurring in natural protein complexes. [30] The strong weight of van der Waals forces and hydrogen bonds revealed that electrostatic contacts, although important, were not the unique actors in the self-assembling of modular monomers. In this context, capsid proteins interact mainly through a combination of electrostatic repulsion, hydrophobic attraction and specific contacts between given pairs of amino acids. These interactions impose a certain restriction in the orientation of the interaction during complex formation, and once this is formed the weaker van der Waals forces complete the assembly. Varying the acidity and salinity conditions (or the concentration of Ca^{2+} ions) adjusts the relative balance between these competing interactions, thereby favouring assembly or disassembly. Electrostatic contacts might be the starting force promoting initial protein-protein contacts in artificial protein nanoparticles, which are later complemented with other type of interactions by slight conformational/spatial adjustments.

Linked to their high functional versatility, proteins (in form of ligands or antibodies) are preferred to functionalize most of the currently developed drug vehicles targeted to specific cell types. [31] In addition, because of the high protein biocompatibility and versatility offered by genetic engineering, protein-only nanoparticles are extremely promising in nanomedicine as they can recruit, apart from cell targeting, a diversity of functions that are appealing in drug delivery such as self-assembling, cage formation, nucleic acid binding, endosomal escape and nuclear transport. [32,33,34] The less desired immunogenicity associated to proteins is expected to be solved by using homologous and biologically inert proteins (such as albumin) as scaffolds for nanoparticle construction. [35] However, protein self-assembling is far from full rational control. This is due to the current inability in linking molecular architecture with the forces that regulate cross-molecular interactions. [30] In fact, the actual complexity that allows correct assembling of viral shells is not reflected by the apparent simplicity of the capsid components and it cannot be predicted in advance from the analysis of the monomers. Here we prove that the assembly promoted by a short cationic peptide (such as R9 or T22) combined with a hexahistidine tail, fused to the end termini of different proteins acting as building blocks, mimic the organization of natural protein complexes such as viral shells, conferring a high stability of the nanoparticle once administered in the bloodstream. Importantly, the efficient tissue targeting combined with absence of renal filtration indicates that R9 and T22 peptides maintain their activities as ligands while

promoting the cross-molecular interactions between monomers in tightly assembled nanoparticles. In the particular case of T22, its targeting to CXCR4+ cells makes this tag not only appealing for drug delivery in colorectal cancer but also in the treatment of other neoplasias (e.g. breast, ovary or prostate cancer or acute myeloid leukaemia),[36] in which high membrane expression of CXCR4 correlates with poor prognosis. Protein nanoparticles displaying effective T22 tags could also be used as vehicles for targeting other diseases in which the pathological mechanisms involve CXCR4 expression, such as pulmonary fibrosis [37] or myocardial infarction. [38]

Since the tags tested here promote self-assembling of structurally diverse proteins such as GFP, [16] p53 [16] and iRFP (the present study), it opens a plethora of opportunities in selecting monomer cores that could be more convenient to avoid immune responses (namely homologous proteins) when administering protein nanoparticles in a clinical context. On the other side, proteins such as p53 with an intrinsic therapeutic value might gain stability and therefore activity when delivered with a particulate organization, in a step beyond the purpose of acting as mere carriers for the delivery of cargo drugs. Although ionic strength appears to be important during nanoparticle organization, this parameter does not affect the stability of already formed particles. This fact allows these entities overcoming biological barriers and reaching their target in a nanoparticulate form. The engineering platform based on the addition of architectonic tags other than oligomerization domains offer a wide and unexpected plasticity in the design of multifunctional modular monomers (a diversity of protein species being suitable as cores), and it opens a spectrum of opportunities for the fully *de novo* design of robust protein-based carriers (artificial viruses) for emerging nanomedical applications.

Conclusions

We have here determined the functional robustness and architectonic stability of fully *de novo* designed protein-only nanoparticles, based on a generic engineering principle in which modular monomers are tagged with end-terminal cationic peptides. A sharp coincidence between nanoparticle formation *in vitro* and the *in vivo* escape from renal filtration has been revealed for several model proteins, proving the maintenance of protein-protein interactions in the bloodstream. Then, the architectonic principles described here offer promise to approach a rational design of self-assembling artificial viruses based on recombinant proteins for nanomedical applications *in vivo*.

Methods

Proteins and protein purification

R9-GFP-H6 and T22-GFP-H6 are modular proteins in which the cationic peptides R9 (nine arginines, [23]) and T22 (derived from polyphemusin II, [20]) are respectively fused to the amino terminus of a hexahistine C-tagged GFP (GFP-H6). These peptides, apart from providing positive charges that create a dipolar building block,[19] confer targeting properties to the resulting nanoparticle. In the case of T22, a ligand of CXCR4,[20] this has been experimentally confirmed as the administered protein accumulates in primary and metastatic foci in a colorectal cancer model.[19] Ang-GFP-H6 and Seq-GFP-H6 are closely related proteins that do not form nanoparticles, since the amino-terminal tags are not cationic.[19] T22-IRFP-H6 was designed in house, and synthetic genes were provided and subcloned into pET22b plasmid vector (using NdeI and HindIII restriction sites) by Genesript (Piscataway, USA). T22-IRFP-H6 has a similar modular scheme than T22-GFP-H6 but in this case, the central part of the fusion was not GFP but the near-infrared fluorescent dimeric protein IRFP. [39] All proteins were encoded by pET22b in *Escherichia coli* Origami B (BL21, OmpT$^-$, Lon$^-$, TrxB, Gor$^-$ (Novagen)), produced overnight at 20 Cº upon 1 mM IPTG addition, and purified by Histidine-tag affinity chromatography as described.[16] In short, we used HiTrap Chelating HP 1 ml columns (GE Healthcare) in an ÄKTA purifier FPLC (GE Healthcare). Cell extracts were disrupted at 1100 psi in a French Press (Thermo FA-078A) and soluble and insoluble fractions separated by centrifugation at 20,000 g for 45 min at 4ºC. The soluble fraction was charged onto HiTrap column and subsequently washed with Tris 20 mM, NaCl 500 mM, Imidazole 10 mM, pH=8 buffer. Proteins were eluted by linear gradient of high Imidazole concentration buffer (20 mM Tris, 500 mM NaCl, 500 mM Imidazole, pH=8). Once in elution buffer, they were dialyzed against the most appropriate buffer regarding stability (empirically determined to minimize unspecific aggregation), which was found to be carbonate buffer (166 mM $NaHCO_3$, pH 7.4) for Ang-GFP-H6, Seq-GFP-H6 and T22-IRFP-H6, Tris NaCl (20 mM Tris, 500 mM NaCl pH 7.4) for T22-GFP-H6 and Tris dextrose (20 mM Tris, 5 % dextrose pH 7.4) for GFP-H6 and R9-GFP-H6. The high salt buffer was always obtained by adding NaCl to reach a final concentration of 500 mM. Once dialyzed, protein samples were stored at -80 ºC until use. Protein integrity was systematically assessed by Western blot analysis, MALDI-TOF and N-terminal sequencing.

Analysis of protein stability

The stability of proteins GFP-H6, R9-GFP-H6, Ang-GFP-H6 and Seq-GFP-H6 was analyzed by measuring fluorescence emission after incubation in different media. R9-GFP-H6 was diluted, in triplicate, in either human serum (Sigma, ref: S2257-5ML, final concentration of 0.23 µg/µl) or in human and mouse plasma (final concentration of 0.11 µg/µl). GFP-H6, Ang-GFP-H6 and Seq-GFP-H6 were also diluted, in duplicate, in the same media, at final concentrations of 0.23, 0.13 and 0.08 µg/µl, respectively. Human blood was obtained from a healthy donor in the Hospital de Sant Pau. Murine blood (approximately 250 µl per mouse) was obtained from the submandibular facial vein of five control mice (25 g) in heparinized tubes. A plasma pool sample was obtained by centrifugation of total blood at 600 g for 10 min at 4ºC. Right after dilution, samples were harvested (time 0) and its fluorescence signal was taken as the initial reference value (100 %). Proteins were further incubated (at 37ºC, in agitation) and samples were taken, at different time points, up to 22 hours. Protein functional stability during incubations was analyzed by fluorescence determination at 510 nm in a Cary Eclipse fluorescence spectrophotometer (Variant, Inc., Palo Alto, C.A) using an excitation wavelength of 450 nm.

Dynamic light scattering

Volume size distribution of nanoparticles and monomeric protein versions were measured using a dynamic light scattering (DLS) analyzer at the wavelength of 633 nm, combined with non-invasive backscatter technology (NIBS) (Zetasizer Nano ZS, Malvern Instruments Limited, Malvern, U.K.). Samples were measured at 20ºC. DLS measurements of solvents were used as controls. The measurements were performed in triplicate.

Fluorescence emission spectra determination

Nanoparticles fluorescence emission spectra from 500 nm to 540 nm was determined by a Cari Eclipse fluorescence spectrophotometer (Variant, Inc., Palo Alto, C.A) using an excitation wavelength of 450nm.

Transmission electron microscopy (TEM)

Droplets of each protein sample (5 µl, 0.150 mg/ml) were deposited in duplicate onto carbon-coated copper grids for 2 min, and excess specimen was then withdrawn. A set of samples was submitted to negative staining with uranyl acetate, whereas the other set was rotary shadowed by evaporation of atomized platinum-carbon at an angle of 25º. Samples were observed with a Jeol 1400 transmission electron microscope (TEM), equipped with a CCD Gatan ES1000W Erlangshen camera.

Cryo transmission electron microscopy (CryoTEM)

Drops of protein solutions (3 µl) were deposited on Quantifoil R 1.2/1.3 grids and blotted to eliminate the excess of sample. Then, grids were plunged in liquid ethane in a Leica EM CPC, placed in a Gatan cryo-transfer specimen holder and observed in a Jeol JEM 2011 transmission electron microscope operating at 200 kV and equipped with a CCD Gatan 895 USC 4000 camera.

Field Emission Scanning Electron Microscopy (FESEM)

To characterize the native morphology and distribution of protein nanoparticles, 5 µl of protein solution samples were deposited into a silicon substrate, and excess of material was then removed. Samples were air dried and observed without coating in a FESEM Zeiss Merlin operating at 2 kV. Images were acquired with a high resolution in-lens secondary electron detector. Image J 1.46n software was used for nanoparticle size distribution analysis in FESEM images.

Atomic force microscopy

Atomic force microscopy (AFM) analyses were performed in liquid with a commercial atomic force microscope (PicoSPM 5100 from Molecular Imaging Agilent Technologies, Inc., Santa Clara, CA, USA) operating in acoustic mode. R9-GFP-H6 in 20 mM Tris buffer pH 7.5 + 5 % dextrose (4 µg/µl, 20 µl) was dropped onto a freshly cleaved mica surface and imaged in liquid. T22-GFP-H6 in sodium bicarbonate 1.4 % buffer pH 7.4, (4.3 µg/µl, 50 µl) were dropped onto a freshly cleaved mica surface and imaged in liquid. For the acoustic mode measurements, a silicon (Applied NanoStructures, Inc.)

tip, with a radius of 10 nm, a nominal spring constant of 0.6–3.7 N/m and a resonance frequency of 43-81 kHz was used.

Size exclusion chromatography

The molecular weight distribution of protein nanoparticles was determined by size exclusion chromatography after injection of 100 µl samples in a previously calibrated Superdex200 10/300 GL (Tricorn) column (GE Healthcare).

Animals and administration regime

Five-week-old female Swiss nu/nu mice weighing between 18 and 20 g (Charles River, L-Abreslle, France), maintained in SPF conditions, were used for *in vivo* studies. All the *in vivo* procedures were approved by the Hospital de Sant Pau Animal Ethics Committee. We assessed, stability, biodistribution and renal clearance of protein constructs 2 hours after i.v. administration of 500 µg/mouse (n=3 mice). The control mice (n=3) were administered i.v. in the appropriate buffer (20 mM Tris, 5 % dextrose pH 7.5 for R9-GFP-H6, 20 mM Tris, 500 mM NaCl pH 7.4 for T22-GFP-H6 and 166 mM $NaC0_3H$ pH 7.5 for Seq- and Ang-empowered constructs). We also assessed the stability and renal clearance of T22-IRFP-H6 dissolved in high salt carbonate buffer (+) or low salt carbonate buffer (-) by i.v. administration of 50 µg/mouse (n=3 mice), 24 hours post-administration. Control mice were administered i.v. with the same buffer. The animal model for metastatic colorectal cancer has been described in detail elsewhere.[19]

Biodistribution of nanoparticles in mice

At 2 hours post administration, mice were anesthetised with isofluorane and whole-body fluorescence was monitored using the IVIS® Spectrum equipment (Xenogen, France). Subsequently, mice blood was collected and necropsy was performed and all organs were removed and placed individually into wells to determine GFP or IRFP fluorescence in an IVIS® Spectrum. Then, these organs were collected, fixed in 4 % formaldehyde in phosphate buffer for 24 hours and finally embedded in paraffin for histological and immunohistochemical evaluation. Nanoparticle biodistribution in blood was determined after centrifugation using a ficoll gradient. In the resulting blood fractions, we registered GFP-derived fluorescence using an IVIS Spectrum. In all

cases, the fluorescence signal was digitalized and after subtracting the autofluorescence, it was displayed as a pseudocolor overlay and expressed in terms of Radiant efficiency for each protein group (control or experimental), dose and time. To calculate half-life of elimination and the elimination rate constant (kel), GFP fluorescence signal was recorded in plasma at time 0, 1, 2, 4, 8 hours after a single 200 µg intravenous dose of R9-GFP-H6 or of T22-GFP-H6.

Histopathology and inmunohistochemistry for GFP-His-tag proteins

Four-micrometer-thick sections were stained with haematoxylin-eosin (H&E) and a complete histopathological analysis was performed by two independent observers. In addition, a quantitation of the number of dead cells, as measured determining apoptotic bodies, in spleen, lung liver, kidney and brain tissues were counted in ten 40x microscopic fields. The presence and location of the GFP-His tagged proteins in tissue sections were demonstrated by inmunohistochemistry. Paraffin-embedded tissue sections (4 µm) were de-paraffinized, re-hydrated and washed in PBS-T. Antigen retrieval was performed by citrate buffer at 120ºC. After quenching peroxidase activity by incubating the slides in 3 % H_2O_2 for 10 min, the slides were washed in PBS-T. Slides were incubated 30 min with a primary antibody against GFP (1:100; St Cruz Biotechnology, Inc. Santa Cruz, CA, USA) or Histidine (1:1000; GE Healthcarhe, UK), washed in PBS-T and incubated with the secondary horseradish peroxidase (HRP) conjugated antibody for 30 min at room temperature. The antibody interaction was then visualized using the chromogenic detection, in which the HRP cleaved the DAB substrate (DAKO, Denmark) to produce a brown precipitate at the location of the protein. Finally sections were counterstained with haematoxylin, dehydrated with decreasing percentages of ethanol (100-95-70-50 %) and mounted using DPX mounting medium. Representative pictures were taken using Cell^B software (Olympus Soft Imaging v 3.3, Japan) at 400 x magnification.

Molecular modeling

Models of R9-GFP-H6 monomers were built using Modeller 9v2 (24) and docked using HADDOCK v 2.0,[40] enforcing C5 symmetry and using N-terminal arginine residues as the active residues (Figure 4). The models were generated using the same protocols previously described.[18] The energetics of the models were analysed with FoldX using the function AnalyseComplex.[41]

Acknowledgment. We appreciate the technical support of Fran Cortés from the Cell Culture Unit of Servei de Cultius Cel.lulars Producció d'Anticossos i Citometria (SCAC, UAB), of Emma Rossinyol from Servei de Microscòpia (UAB), and of Amable Bernabé from Soft Materials Service (ICMAB-CSIC/CIBER-BBN). We are also indebted to the Nanotoxicology Platform and Protein Production Platform (http://www.bbn.ciber-bbn.es/programas/plataformas/equipamiento). The authors also acknowledge the financial support granted to E.V. (PI12/00327) and R.M. (PI12/01861) from FIS, to A.V. and J. V. from Agència de Gestió d'Ajuts Universitaris i de Recerca (grants 2009SGR-108 to A.V., SGR2009-516 to J.V. and 2009-SGR-1437 to R.M.), to R.M. and to A.V. from La Marató de TV3 (416/C/2013), to J.V. from DGI (grant CTQ2010-19501) and from the Centro de Investigación Biomédica en Red (CIBER) de Bioingeniería, Biomateriales y Nanomedicina (NANOPROVIR, NANOCOMETS and PROGLIO projects), financed by the Instituto de Salud Carlos III with assistance from the European Regional Development Fund. U.U. received a fellowship grant from ISCIII. W.T. is grateful to the Consejo Superior de Investigaciones Científicas (CSIC) for a "JAE-pre" fellowship. A.V. has been distinguished with an ICREA ACADEMIA Award.

Supporting Information Available: Wider AFM fields, biodistribution of nanoparticles and control proteins in blood cells, analysis of nanoparticle toxicity *in vivo* and stability in blood. This material is available free of charge *via* the Internet at http://pubs.acs.org.

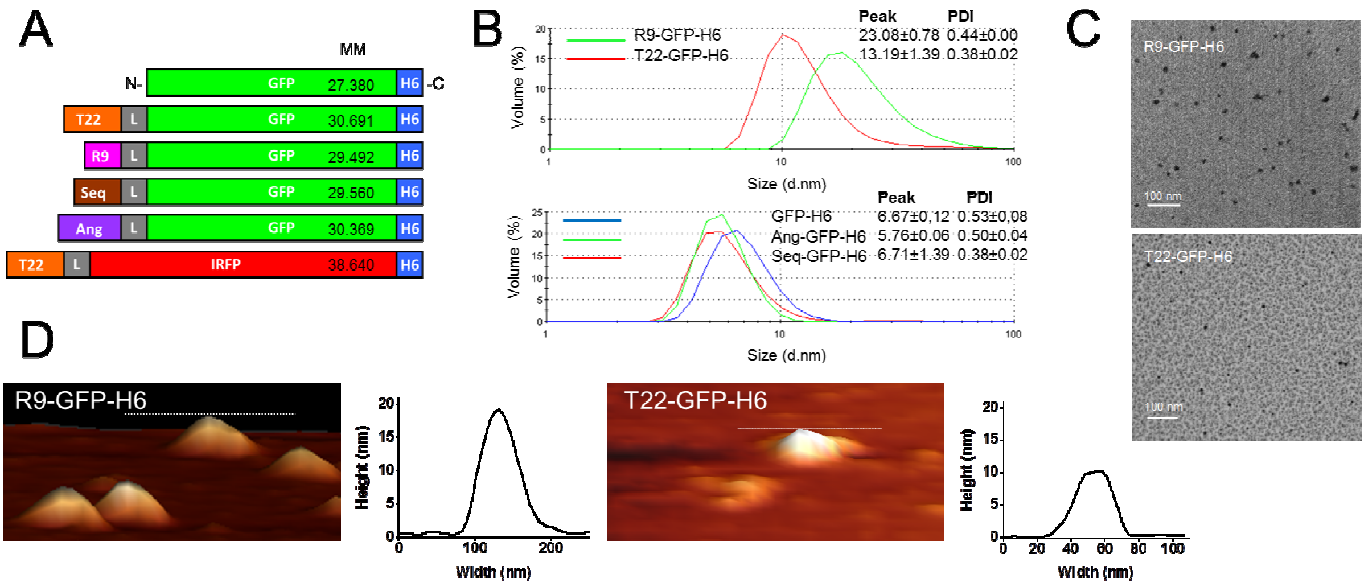

Figure 1. *In vitro* assembling of protein-only nanoparticles. A) Schematic representation of all protein constructs used in the study. Precise amino acid sequences of R9, T22, Ang (Angiopep-2) and Seq (Seq-1) have been given elsewhere.[18,19] L is a linker peptide commonly used in phage display (GGSSRSS). [42] The molecular masses (MM) of proteins were determined by mass spectroscopy and they were coincident with predicted values. B) Size of protein complexes formed by distinct GFP variants, measured by DLS in representative experiments. Peak and polydispersion index (PDI) are shown for each plot. C) TEM images of protein nanoparticles upon purification from producing bacteria. D) AFM images of randomly selected nanoparticles and topography cross-sections of isolated entities. Measurements have been done in liquid with a tip radius of 10 nm. Then, the width (but not the high) of the particles is inherently overestimated.

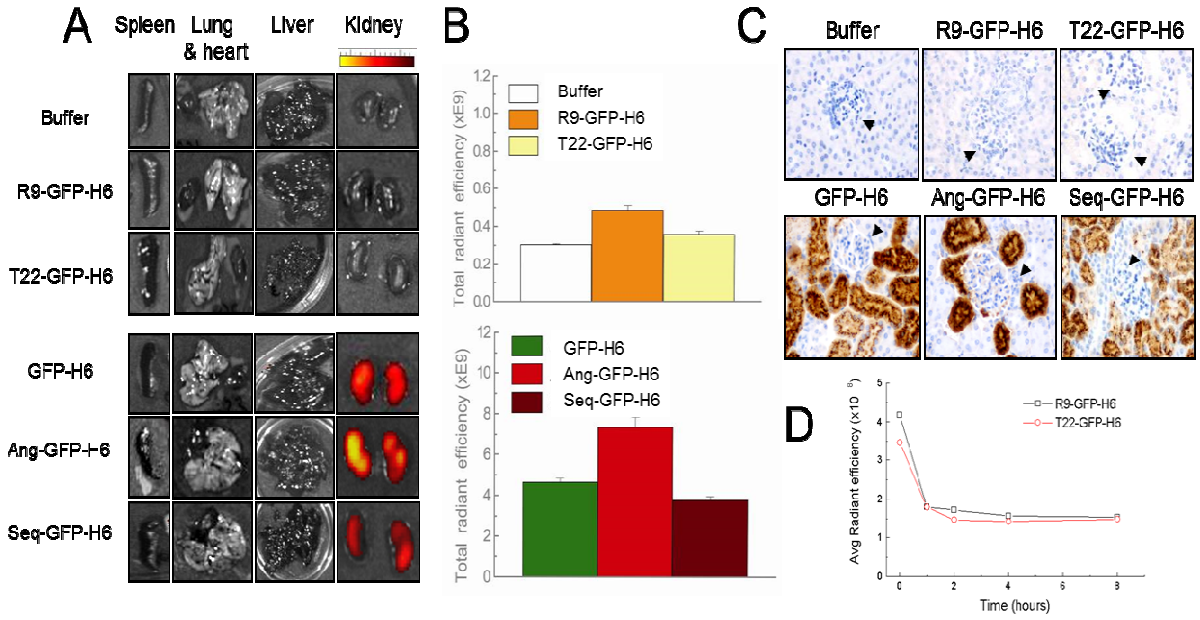

Figure 2. Stability and biodistribution of protein constructs. A) GFP signal registered *ex vivo* in mouse spleen, lung, heart, liver sections and kidneys 2 hours after i.v. administration of 500 µg of each protein or buffer alone. B) Quantitative determination of fluorescence in analysed kidneys expressed as the total radiant efficiency (ph/sec/cm2/sr/µW/cm2) of right and left kidneys for each mouse. The slight variations found when comparing proteins could be due to differences in the specific fluorescence, as protein sizes are rather similar (Figure 1). C) Imnunohistochemical anti-GFP detection of the administered proteins in the renal tissue, which is only observed if the small size (< 7 nm) of the administered material determines its filtration and accumulation in the renal glomeruli while being excreted (400 x magnification). Arrowheads show high density of haematoxylin stained nuclei (blue) corresponding to cells in the renal tissue, including glomerular cells. Note the absence of GFP staining in animals administered with R9- and T22-containing proteins, and the presence of signal when Ang- and Seq-derived proteins were administered (brown staining). D) Pharmacokinetics of R9-GFP-H6 and T22-GFP-H6 after a 200 µg intravenous bolus administration. GFP fluorescence was recorded in plasma obtained after blood centrifugation at time 0, 1, 2, 4, 8 hours. The elimination rate constant (Kel), and half-life of elimination (t1/2), were calculated using a one-compartment model and a semi-log plot of plasma concentration *versus* time curve (see Supplemental Table 1). R9-GFP-H6 and T22-GFP-H6 showed a fast distribution in the blood compartment followed by a slow half-life of recirculation in blood.

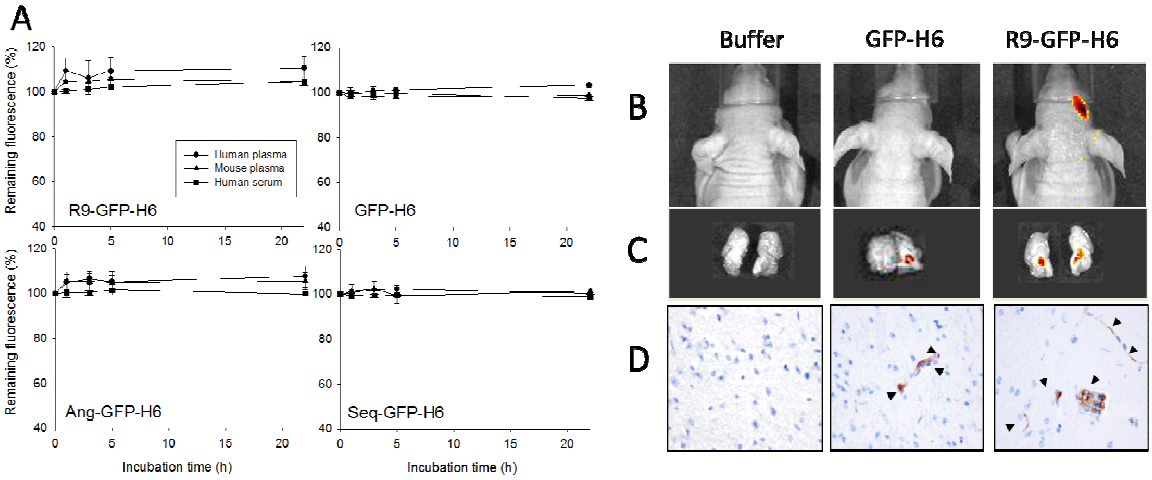

Figure 3. Stability and biodistribution of R9-GFP-H6. A) *In vitro* stability of protein R9-GFP-H6 and control proteins GFP-H6, Ang-GFP-H6 and Seq-GFP-H6 in human plasma (circles), mouse plasma (triangles) and human serum (squares), monitored by fluorescent emission.B) *In vivo* whole-body recording of a representative mouse 2 hours after i.v. administration with buffer alone, with 500 µg of GFP-H6 or R9-GFP-H6, showing occurrence of fluorescence in the brain. C) GFP fluorescence signal recording in *ex vivo* brain sagittal sections of a representative mouse. D) Inmunohistochemical detection of the protein using and anti-GFP antibody, in mouse brain sections 2 hours after i.v. administration of 500 µg of GFP-H6 and R9-GFP-H6 of buffer alone (400x). Arrows show protein accumulation in the brain parenchyma.

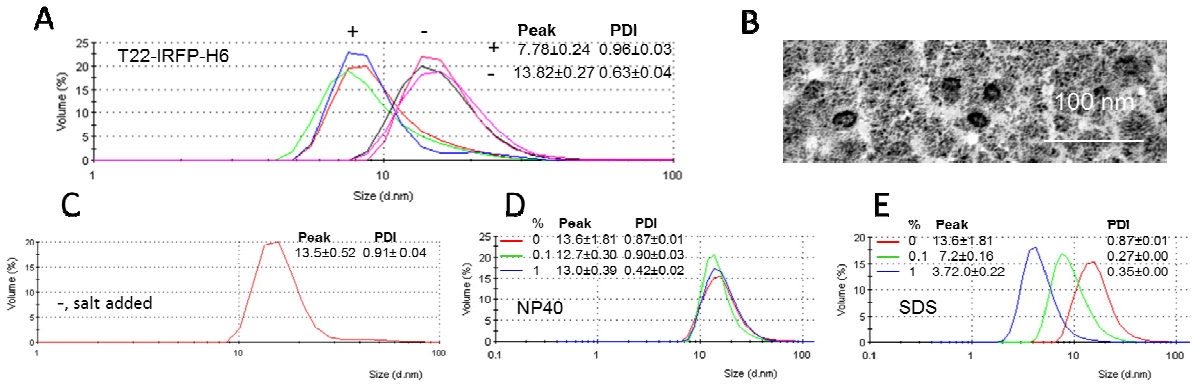

Figure 4. Structural memory of protein-only nanoparticles *in vitro*. A) DLS size analysis of T22-IRFP-H6 purified in low salt (carbonate buffer, -) and high salt (carbonate buffer + 334 mM NaCl, +). Different measures are plotted to evidence robustness of data. B) TEM analysis of T22-IRFP-H6 purified in low salt buffer (assembled). C) DLS size analysis of T22-IRFP-H6 purified in low salt buffer and in which additional salt was added later to reach 500 mM NaCl. Alternatively, NP40 (D) and SDS (E) were added up to 1 %. Peak and PDI values are shown for each DLS plot.

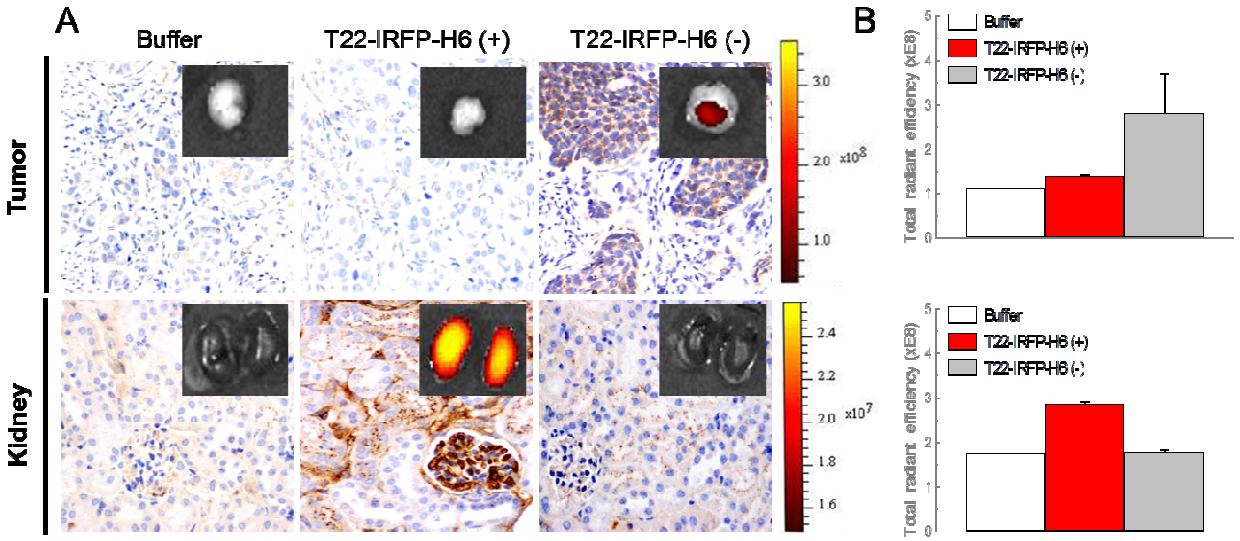

Figure 5. Structural memory of protein-only nanoparticles *in vivo.* Mouse tumor and kidney sections were registered 24 hours after 50 µg i.v. administration of T22-IRFP-H6 in either high (+, disassembled) or low (-, assembled) salt buffers. A) Immunohistochemical analysis of the tumor and glomeruli using an anti His-tag antibody (400X magnification). Insets show IRFP fluorescence signal detected *ex vivo* in tissues of a representative mouse for each group, after subtracting the autofluorescence. B) The total radiant efficiency (ph/sec/cm^2/sr/µW/cm^2) as determined for each group in tumour (top) and kidney (bottom).

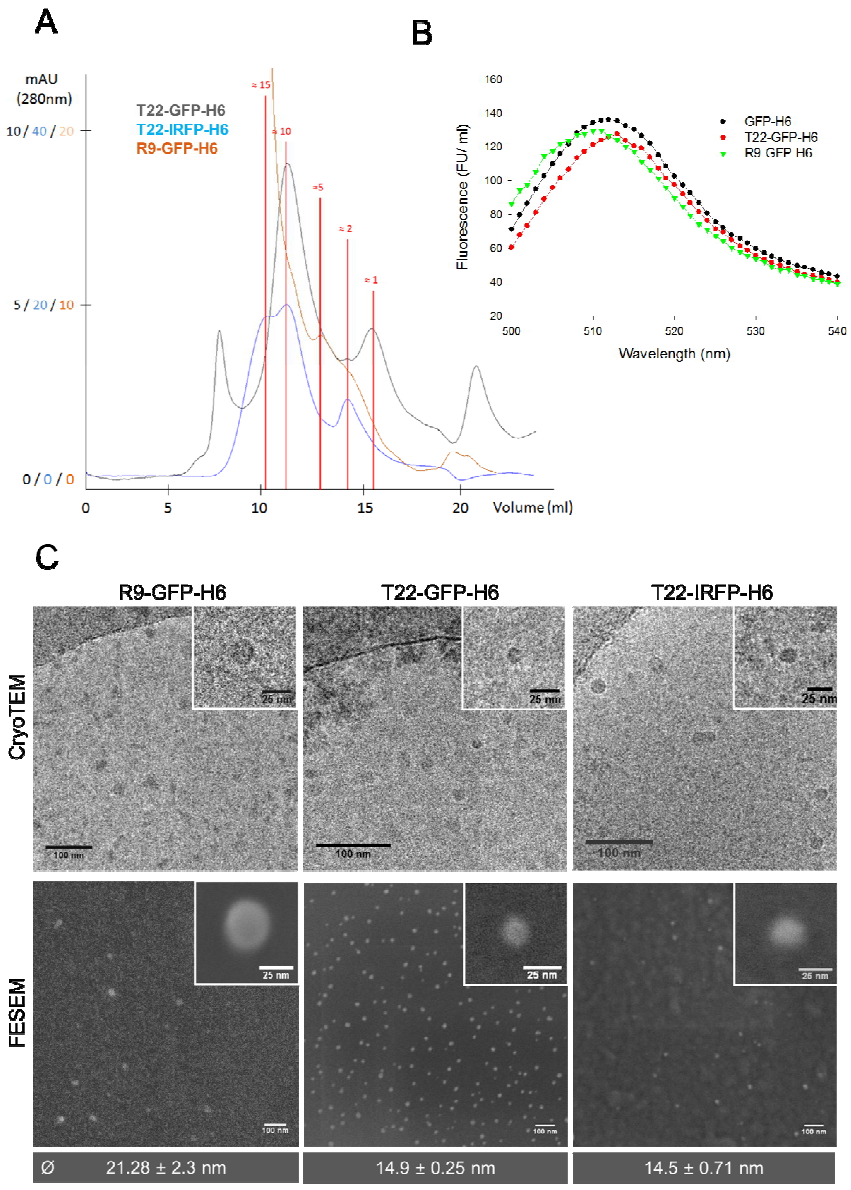

Figure 6. Fine architecture of protein-only nanoparticles. A) Overlap of size exclusion chromatograms of different protein nanoparticles. Vertical red lines indicate the occurrence of nanoparticles by the position of peaks, indicating the estimated number of monomers that form them. B) Overlap of fluorescence emission spectra of assembled protein nanoparticles (T22-GFP-H6, R9-GFP-H6) compared with that of the monomeric control protein (GFP-H6). C) A) Wide field CryoTEM and FESEM images of protein nanoparticles formed by different proteins. The average size of each type of particle was determined by SEM and depicted. The insets show magnifications of single nanoparticles.

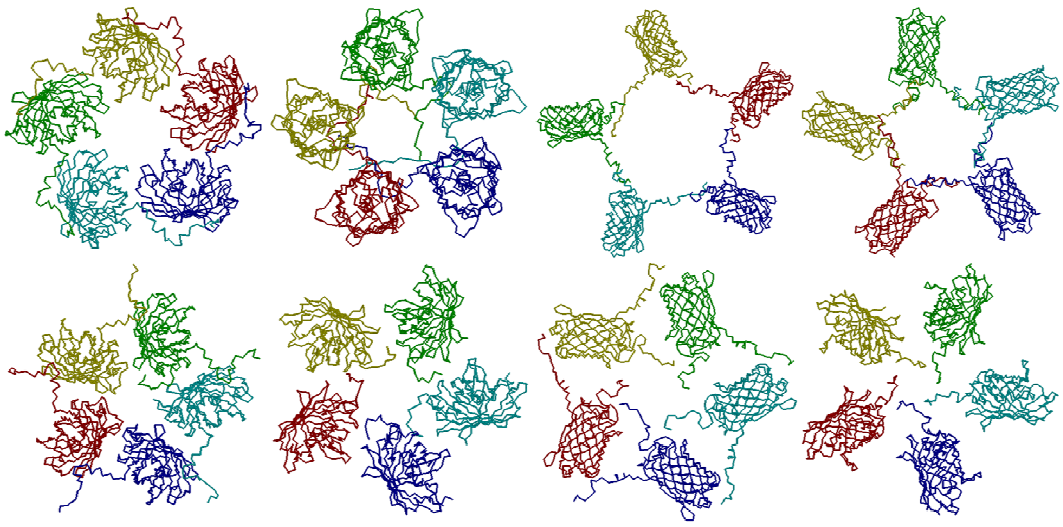

Figure 7. Different conformations of R9-GFP-H6 nanoparticles obtained in the docking process by using different configurations of overhanging R9 and H6 peptides. Models in the top row, were generated with HADDOCK [40] using R9 residues as active and H6 residues as passive. Models in the bottom row were generated declaring only R9 residues as active. The energetics governing protein-protein interactions in each of these models are given in Table 1.

Table 1. Summary of energetics governing monomer-monomer interactions in the molecular models depicted in Figure 4.

Model [a]	Hydrogen bond [b]	Van der Waals [b]	Electrostatics [b]
UP 1	-47,34	-65	-21,56
UP 2	-44,97	-57,16	-6,61
UP 3	-29,13	-42,38	-7,33
UP 4	-31,6	-38,18	-10,85
DOWN 1	-26,45	-30,56	2,86
DOWN 2	-23,13	-25,79	-4,6
DOWN 3	-12,64	-20,78	1,02
DOWN 4	-7,57	-11,83	12,21

[a] Models refer to those depicted in Figure 7, in top and bottom rows, numbered from left to right.

[b] Values were calculated with FoldX and are given in kcal/mol.

References

1 Villaverde A *Nanoparticles in Translational Science and Medicine*; Academic Press (Elsevier): London, 2011.

2 Sharifi, S.; Behzadi, S.; Laurent, S.; Forrest, M. L.; Stroeve, P.; Mahmoudi, M. Toxicity of Nanomaterials. *Chem. Soc. Rev.* **2012,** *41,* 2323-2343.

3 Giacca, M.; Zacchigna, S. Virus-Mediated Gene Delivery for Human Gene Therapy. *J. Control Release* **2012,** *161,* 377-388.

4 Edelstein, M. L.; Abedi, M. R.; Wixon, J. Gene Therapy Clinical Trials Worldwide to 2007--an Update. *J. Gene Med.* **2007,** *9,* 833-842.

5 Ma, Y.; Nolte, R. J.; Cornelissen, J. J. Virus-Based Nanocarriers for Drug Delivery. *Adv. Drug Deliv. Rev.* **2012,** *64,* 811-825.

6 Corchero, J. L.; Cedano, J. Self-Assembling, Protein-Based Intracellular Bacterial Organelles: Emerging Vehicles for Encapsulating, Targeting and Delivering Therapeutical Cargoes. *Microb Cell Fact.* **2011,** *10,* 92.

7 Rome, L. H.; Kickhoefer, V. A. Development of the Vault Particle As a Platform Technology. *ACS Nano.* **2012**.

8 Zlotnick, A. Are Weak Protein-Protein Interactions the General Rule in Capsid Assembly? *Virology* **2003,** *315,* 269-274.

9 Lakshmanan, A.; Zhang, S.; Hauser, C. A. Short Self-Assembling Peptides As Building Blocks for Modern Nanodevices. *Trends Biotechnol* **2012,** *30,* 155-165.

10 Doll, T. A.; Raman, S.; Dey, R.; Burkhard, P. Nanoscale Assemblies and Their Biomedical Applications. *J. R. Soc. Interface* **2013,** *10,* 20120740.

11 Lai, Y. T.; Cascio, D.; Yeates, T. O. Structure of a 16-Nm Cage Designed by Using Protein Oligomers. *Science* **2012,** *336,* 1129.

12 Bai, Y.; Luo, Q.; Zhang, W.; Miao, L.; Xu, J.; Li, H.; Liu, J. Highly Ordered Protein Nanorings Designed by Accurate Control of Glutathione S-Transferase Self-Assembly. *J. Am. Chem Soc.* **2013,** *135,* 10966-10969.

13 Yang, Y.; Burkhard, P. Encapsulation of Gold Nanoparticles into Self-Assembling Protein Nanoparticles. *J. Nanobiotechnology.* **2012,** *10,* 42.

14 King, N. P.; Sheffler, W.; Sawaya, M. R.; Vollmar, B. S.; Sumida, J. P.; Andre, I.; Gonen, T.; Yeates, T. O.; Baker, D. Computational Design of Self-Assembling Protein Nanomaterials With Atomic Level Accuracy. *Science* **2012,** *336,* 1171-1174.

15 Usui, K.; Maki, T.; Ito, F.; Suenaga, A.; Kidoaki, S.; Itoh, M.; Taiji, M.; Matsuda, T.; Hayashizaki, Y.; Suzuki, H. Nanoscale Elongating Control of the

Self-Assembled Protein Filament With the Cysteine-Introduced Building Blocks. *Protein Sci.* **2009,** *18,* 960-969.

16 Unzueta, U.; Ferrer-Miralles, N.; Cedano, J.; Zikung, X.; Pesarrodona, M.; Saccardo, P.; Garcia-Fruitos, E.; Domingo-Espin, J.; Kumar, P.; Gupta, K. C. *et al.* Non-Amyloidogenic Peptide Tags for the Regulatable Self-Assembling of Protein-Only Nanoparticles. *Biomaterials* **2012,** *33,* 8714-8722.

17 Vazquez, E.; Cubarsi, R.; Unzueta, U.; Roldan, M.; Domingo-Espin, J.; Ferrer-Miralles, N.; Villaverde, A. Internalization and Kinetics of Nuclear Migration of Protein-Only, Arginine-Rich Nanoparticles. *Biomaterials* **2010,** ***31,*** 9333-9339.

18 Vazquez, E.; Roldan, M.; Diez-Gil, C.; Unzueta, U.; Domingo-Espin, J.; Cedano, J.; Conchillo, O.; Ratera, I.; Veciana, J.; Daura, X. *et al*. Protein Nanodisk Assembling and Intracellular Trafficking Powered by an Arginine-Rich (R9) Peptide. *Nanomedicine. (Lond)* **2010,** *5,* 259-268.

19 Unzueta, U.; Cespedes, M. V.; Ferrer-Miralles, N.; Casanova, I.; Cedano JA; Corchero JL; Domingo-Espin, J.; Villaverde A; Mangues, R.; Vazquez E Intracellular $CXCR4^{+}$ Cell Targeting With T22-Empowered Protein-Only Nanoparticles. *Int. J. Nanomedicine* **2012,** *7,* 4533-4544.

20 Murakami, T.; Zhang, T. Y.; Koyanagi, Y.; Tanaka, Y.; Kim, J.; Suzuki, Y.; Minoguchi, S.; Tamamura, H.; Waki, M.; Matsumoto, A. *et al*. Yamamoto, N. Inhibitory Mechanism of the CXCR4 Antagonist T22 Against Human Immunodeficiency Virus Type 1 Infection. *J. Virol*. **1999,** *73,* 7489-7496.

21 Feng, B.; LaPerle, J. L.; Chang, G.; Varma, M. V. Renal Clearance in Drug Discovery and Development: Molecular Descriptors, Drug Transporters and Disease State. *Expert. Opin. Drug Metab Toxicol*. **2010,** *6,* 939-952.

22 Kumar, P.; Wu, H.; McBride, J. L.; Jung, K. E.; Kim, M. H.; Davidson, B. L.; Lee, S. K.; Shankar, P.; Manjunath, N. Transvascular Delivery of Small Interfering RNA to the Central Nervous System. *Nature* **2007,** *448,* 39-43.

23 Saccardo, P.; Villaverde, A.; Gonzalez-Montalban, N. Peptide-Mediated DNA Condensation for Non-Viral Gene Therapy. *Biotechnol. Adv.* **2009,** *27,* 432-438.

24 Moghimi, S. M.; Hunter, A. C. Capture of Stealth Nanoparticles by the Body's Defences. *Crit Rev. Ther. Drug Carrier Syst.* **2001,** *18,* 527-550.

(5 Moghimi, S. M.; Hunter, A. C.; Murray, J. C. Long-Circulating and Target-Specific Nanoparticles: Theory to Practice. *Pharmacol. Rev.* **2001,** *53,* 283-318.

26 Ferrer-Miralles, N.; Rodriguez-Carmona, E.; Corchero, J. L.; Garcia-Fruitos, E.; Vazquez, E.; Villaverde, A. Engineering Protein Self-Assembling in Protein-Based Nanomedicines for Drug Delivery and Gene Therapy. *Crit Rev. Biotechnol.* **2013,** *10.3109/07388551.2013.833163 [doi]*, Oct 9, [Epub ahead of print].

27 Unzueta, U.; Saccardo, P.; Domingo-Espin, J.; Cedano, J.; Conchillo-Sole, O.; Garcia-Fruitos, E.; Cespedes, M. V.; Corchero, J. L.; Daura, X.; Mangues, R. *et*

al. Sheltering DNA in Self-Organizing, Protein-Only Nano-Shells As Artificial Viruses for Gene Delivery. *Nanomedicine* **2014**, *10*, 535-541.

28 Heyda, J.; Mason, P. E.; Jungwirth, P. Attractive Interactions Between Side Chains of Histidine-Histidine and Histidine-Arginine-Based Cationic Dipeptides in Water. *J. Phys. Chem. B* **2010,** *114,* 8744-8749.

29 Vondrasek, J.; Mason, P. E.; Heyda, J.; Collins, K. D.; Jungwirth, P. The Molecular Origin of Like-Charge Arginine-Arginine Pairing in Water. *J. Phys. Chem. B* **2009,** *113,* 9041-9045.

30 Leckband, D. Measuring the Forces That Control Protein Interactions. *Annu. Rev. Biophys. Biomol. Struct.* **2000,** *29,* 1-26.

31 Mout, R.; Moyano, D. F.; Rana, S.; Rotello, V. M. Surface Functionalization of Nanoparticles for Nanomedicine. *Chem. Soc. Rev.* **2012,** *41,* 2539-2544.

32 Aris, A.; Feliu, J. X.; Knight, A.; Coutelle, C.; Villaverde, A. Exploiting Viral Cell-Targeting Abilities in a Single Polypeptide, Non-Infectious, Recombinant Vehicle for Integrin-Mediated DNA Delivery and Gene Expression. *Biotechnol Bioeng* **2000,** *68,* 689-696.

33 Vazquez, E.; Ferrer-Miralles, N.; Mangues, R.; Corchero, J. L.; Schwartz S Jr; Villaverde, A. Modular Protein Engineering in Emerging Cancer Therapies. *Curr. Pharm. Des* **2009,** *15,* 893-916.

34 Vazquez, E.; Ferrer-Miralles, N.; Villaverde, A. Peptide-Assisted Traffic Engineering for Nonviral Gene Therapy. *Drug Discov. Today* **2008,** *13,* 1067-1074.

35 Elzoghby, A. O.; Samy, W. M.; Elgindy, N. A. Albumin-Based Nanoparticles As Potential Controlled Release Drug Delivery Systems. *J. Control Release* **2012,** *157,* 168-182.

36 Balkwill, F. The Significance of Cancer Cell Expression of the Chemokine Receptor CXCR4. *Semin. Cancer Biol.* **2004,** *14,* 171-179.

37 Xu, J.; Mora, A.; Shim, H.; Stecenko, A.; Brigham, K. L.; Rojas, M. Role of the SDF-1/CXCR4 Axis in the Pathogenesis of Lung Injury and Fibrosis. *Am. J. Respir. Cell Mol. Biol.* **2007,** *37,* 291-299.

38 Frangogiannis, N. G. The Stromal Cell-Derived Factor-1/CXCR4 Axis in Cardiac Injury and Repair. *J. Am. Coll. Cardiol.* **2011,** *58,* 2424-2426.

39 Filonov, G. S.; Piatkevich, K. D.; Ting, L. M.; Zhang, J.; Kim, K.; Verkhusha, V. V. Bright and Stable Near-Infrared Fluorescent Protein for *in Vivo* Imaging. *Nat. Biotechnol.* **2011,** *29,* 757-761.

40 Dominguez, C.; Boelens, R.; Bonvin, A. M. HADDOCK: a Protein-Protein Docking Approach Based on Biochemical or Biophysical Information. *J. Am. Chem. Soc.* **2003,** *125,* 1731-1737.

41 Guerois, R.; Nielsen, J. E.; Serrano, L. Predicting Changes in the Stability of Proteins and Protein Complexes: a Study of More Than 1000 Mutations. *J. Mol. Biol.* **2002,** *320,* 369-387.

42 Andris-Widhopf, J.; Steinberger, P.; Fuller, R.; Rader, C.; Barbas, C. F., III Generation of Human Fab Antibody Libraries: PCR Amplification and Assembly of Light- and Heavy-Chain Coding Sequences. *Cold Spring Harb. Protoc.* **2011,** *2011.*